Review of Selected RHESSI Solar Results

Brian R. Dennis[1], Hugh S. Hudson[2], and Säm Krucker[2]

[1] NASA Goddard Space Flight Center, Solar Physics Branch, Code 612.1, Greenbelt, MD 20771, USA Brian.R.Dennis@nasa.gov
[2] Space Sciences Laboratory, University of California, Berkeley, CA 94720, USA hhudson@ssl.berkeley.edu krucker@ssl.berkeley.edu

Abstract

We review selected science results from RHESSI solar observations made since launch on 5 February 2002. A brief summary of the instrumentation is given followed by a sampling of the major science results obtained from the soft X-ray, hard X-ray, and gamma-ray energy domains. The thermal continuum measurements and detection of Fe-line features are discussed as they relate to parameters of the thermal flare plasma for several events, including microflares. Observations of X-ray looptop, and rising above-the-loop sources are discussed as they relate to standard models of eruptive events and the existence of a current sheet between the two. Hard X-ray spectra and images of footpoints and coronal sources are presented, showing how they can be used to separate thermal and nonthermal sources and determine the magnetic reconnection rate. Gamma-ray line images and spectra are presented as they relate to determining the location, spectra, and angular distribution of the accelerated ions and the temperature of the chromospheric target material. Finally, we discuss the overall energy budget for two of the larger events seen with RHESSI.

1 Introduction

With its broad energy coverage from 3 keV to 17 MeV, the Reuven Ramaty High Energy Solar Spectroscopic Imager (RHESSI) is providing definitive observations of the three major components of solar flares: plasma at $\geq$10 MK, electrons accelerated to $\geq$10 keV, and ions to $\geq$1 MeV. During a large flare, thermal bremsstrahlung from heated plasma dominates the observed soft X-ray emission to energies often as high as a few tens of keV; nonthermal bremsstrahlung continuum from accelerated electrons is observed at higher, hard X-ray (and sometimes gamma-ray) energies; and line emission from nuclear transitions caused by accelerated ions is observed in gamma-rays from

∼400 keV to ∼8 MeV. In all of these spectral domains, RHESSI has superior capabilities compared to previous instruments. In each case, new and interesting results have already been obtained and many more are promised as the knowledge of the instrument improves, the analysis software is extended to fully exploit RHESSI's imaging spectroscopy capabilities, and observations of the over 14,000 flares recorded to date are fully interpreted.

The impact of the RHESSI observations has been greatly amplified by the contemporaneous observations made with the vast array of other solar instruments currently in operation. These include observations over a broad spectrum of wavelengths from soft X-rays, EUV, UV, and optical, to radio. They provide thermal, magnetic, and morphological context information that is indispensable for the interpretation of the RHESSI observations. Combined with the in situ particle and field measurements in the near-Earth environment, they also provide information on coronal mass ejections (CMEs), the other great energetic solar phenomenon that is often, but not always, associated with flares.

In this review, we summarize some of the early results obtained with RHESSI from its first two years in orbit. The paper is organized by energy into the basic domains of soft X-rays from about 3 to 20 keV, hard X-rays from about 20 to 400 keV, and gamma-rays from about 400 keV to 17 MeV. These roughly correspond to the energy ranges dominated by emissions from thermal plasma, nonthermal electrons, and nonthermal ions, respectively, but there are clearly some overlaps in these interpretations as will become evident in the different sections of the paper.

2 Instrumentation

As described more fully by Lin et al. (2002), RHESSI is a single instrument mounted on a spinning spacecraft with the spin axis pointed close (within ∼10 arc minutes) to the center of the solar disk. The instrument consists of an X-ray/gamma-ray spectrometer that views the Sun through a set of modulation collimators. The spectrometer has nine cylindrical germanium detectors, each 7.1 cm in diameter and 8.5 cm long. They detect photons from 3 keV to 17 MeV with fine energy resolution varying from ∼1 keV (FWHM) at the low energy end to ∼4 keV at 2 MeV. Above each detector sits a modulation collimator made up of two identical grids separated from one another by 1.55 m. All the grids consist of parallel slats separated by slits of comparable width. All the grid slats are tungsten except for those on the finest grid pair, which are molybdenum. As the spacecraft rotates at ∼15 rpm, the modulation collimators convert the spatial information about the source that is contained in the photon arrival directions into temporal modulation of the germanium detector counting rates. Smith et al. (2002) and Hurford et al. (2002) describe how the resulting telemetered energy and timing information about each photon recorded in all nine detectors is used on the ground with

specialized analysis software (Schwartz et al. 2002) to give RHESSI its imaging spectroscopy capabilities. Angular resolutions as fine as 2 arc seconds are possible, and sources as large as 180 arc seconds can be imaged anywhere on the solar disc and up to several arc minutes above the limb. Several innovations have been incorporated into the instrument design to increase the dynamic range of flare intensities that can be recorded with RHESSI so that weak microflares are detected at times of low activity while detector saturation and spectral distortion are minimized during the most intense gamma-ray line flares. These innovations include detector segmentation, movable shutters, and high-rate electronics with pile-up suppression (Smith et al. 2002).

3 Soft X-rays

The soft X-ray spectral range from RHESSI's low energy limit of ∼3 keV to about 20 keV is of great interest since, in many flares, it is the region of transition from thermal to nonthermal emission. Thermal bremsstrahlung continuum and line emissions are seen in this energy range from flare plasmas with temperatures as low as ∼7 MK and as high as many tens of MK. Studying this thermal component can reveal not just the total energy in the hottest flare plasma throughout the flare but also information about the composition of the plasma, its density, and possibly any departure from ionization equilibrium. Nonthermal X-ray emission with a flatter power-law spectrum ($\epsilon^{-\gamma}$ where ϵ is the photon energy) is also seen above ∼10 keV, particularly during the impulsive phase of a flare, from electrons accelerated to tens of keV and higher. Many observations have shown that these accelerated electrons carry a large fraction of the total energy released in many flares, thus heightening the interest in the nonthermal component. Because these accelerated electrons have a steep power-law energy distribution ($E^{-\delta}$ where E is the electron energy) with δ generally >2, most of the energy resides in the lower energy electrons. Indeed, for such a steep power-law spectrum, a lower energy flattening or cutoff must exist to keep the total nonthermal energy finite. The determination of the cutoff energy is critical for any evaluation of flare energetics.

The RHESSI instrument provides much higher sensitivity in the soft X-ray energy range above ∼3 keV than has previously been available. Earlier solar hard X-ray instruments, such as the Hard X-ray Burst Spectrometer (HXRBS) on the Solar Maximum Mission (SMM) and the Hard X-ray Telescope (HXT) on Yohkoh, had entrance windows that absorbed emission below ∼15-25 keV to avoid saturation from the intense thermal emissions in large flares. RHESSI accommodates medium and large flares by automatically inserting shutters (aluminum discs) in front of detectors to absorb low energy solar photons and hence avoid saturation. Thus, when no shutters are in the detector lines of sight to the Sun, RHESSI is about 100 times more sensitive than previous instruments at around 10 keV. Even with the shutters in front of the detectors

during the largest flares, thin areas in the aluminum discs forming the shutters allow small fractions of the photons to pass through, making spectroscopy still possible down to about 5 keV.

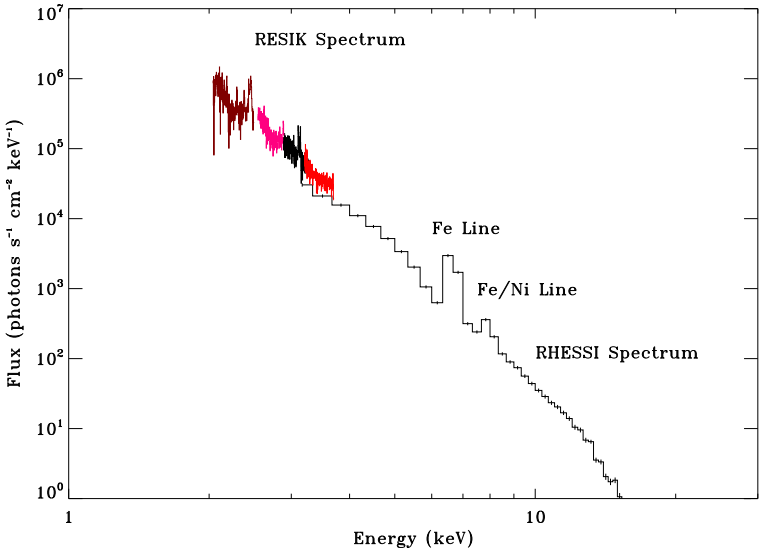

Fig. 1. X-ray spectra determined from RESIK and RHESSI observations for a time (03:00 UT) just preceding the main M2 flare on 2003 April 26. A temperature of 18.6 MK and an emission measure of 2×10^{47} cm^{-3} are obtained from a fit to the RHESSI spectrum assuming the existence of two line complexes with Gaussian profiles. (From Dennis et al. 2005.)

3.1 Thermal Plasma

RHESSI observes emission from thermal plasma with temperatures above ∼7 MK. This includes thermal free-free and free-bound continua plus line emission, primarily from highly ionized iron and nickel. The continuum, with its pseudo-exponential shape, allows RHESSI to provide accurate determinations of the emission measure $EM = \int N_e^2 \, dV$ (where N_e is the electron density and V is the emitting volume) and temperature T assuming an isothermal plasma. Differential emission measure analysis is also possible by combining RHESSI data with observations from other instruments in different wavelength ranges. With its ∼1-keV FWHM energy resolution, RHESSI does not resolve the satellite-line structure of the Fe and Ni lines between ∼6.4 and 10 keV described by Phillips (2004). Instead, it sees two broad Gaussian-like features when the plasma temperature is ≥10 MK, one centered at ∼6.7 keV and the other weaker feature at ∼8 keV. These features are made up of a large

number of FeXXV lines and FeXXIV dielectronic satellites, with other lines due to FeXXVI and Ni XXVII contributing at higher temperatures. Such a spectrum is shown in Fig. 1, where data from the RESIK Bragg crystal spectrometer (Sylwester et al. 2004) on the Russian *CORONAS-F* spacecraft have been added to the spectrum derived from RHESSI observations for the early stages of an M2 flare seen by both instruments on 2003 April 26.

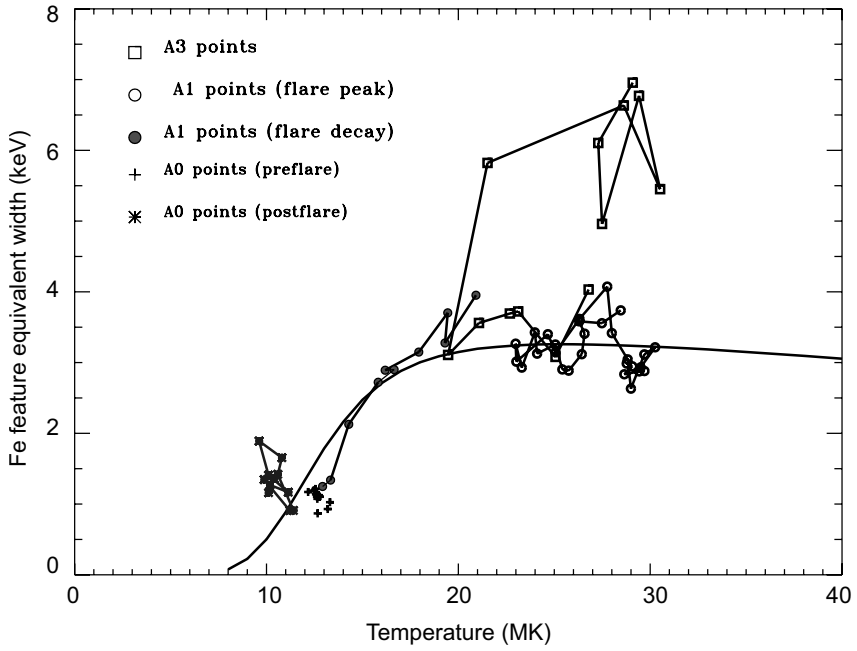

Fig. 2. Equivalent width (keV) of the Fe line feature at 6.7 keV plotted against T (smooth curve) as calculated from CHIANTI assuming coronal abundances, i.e. Fe/H and Ni/H equal to 4× photospheric, and Mazzotta et al. (1998) ion fractions. Observed *RHESSI* values in attenuator states A0, A1, and A3 for the M2 flare of 2003 April 26 are shown as points connected by lines (see legend for line styles and plotting symbols). (From Dennis et al. 2005.)

The two line features in the RHESSI spectra provide information on the plasma temperature and iron abundance that is independent of similar information derived from the continuum. A convenient way of expressing the intensities of the two line features is through the equivalent width, i.e. the energy width of a portion of the continuum at the line's energy with flux equal to that of the line feature. The variation of equivalent width with T is given in Fig. 2 (smooth curve) based on CHIANTI version 5 (Dere et al. 1997), with "coronal" element abundances ([Fe/H] $\sim 1.6 \times 10^{-4}$) and recent ion fraction calculations. This should be compared with values determined from RHESSI

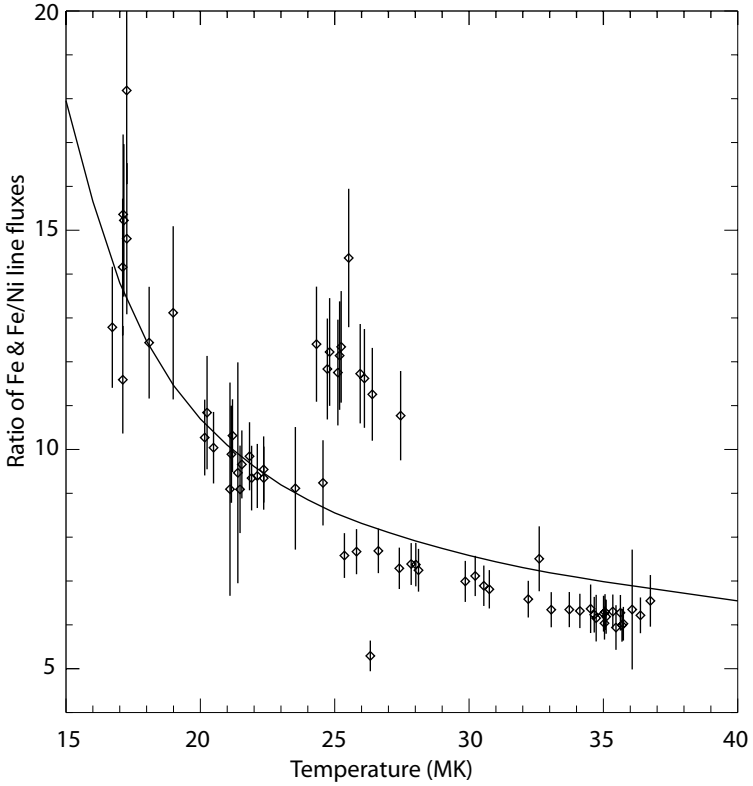

Fig. 3. Results of RHESSI spectral analysis showing the ratio of the Fe to Fe/Ni line fluxes at 6.7 and 8 keV, respectively, plotted as a function of the plasma temperature derived from the continuum assuming a single temperature (from Caspi et al. 2004). The uncertainties on the temperatures are of the order of 1 MK. The solid curve is the predicted variation from CHIANTI assuming ionization fractions given by Mazzotta et al. (1998). Data points are for the X4.8 gamma-ray line flare observed on 2002 July 23 starting at 00:18 UT in various attenuator states.

spectra similar to that shown in Fig. 1 for the flare on 2003 April 26. As can be seen, for observations in the A1 attenuator states (thin shutters in place over the detectors) on the rise and decay of the flare, the observed equivalent widths of the Fe-line feature lie close to the theoretical curve, giving support for a coronal abundance of Fe in the flare plasma. However, some of the equivalent widths measured in the A3 attenuator state (both thick and thin attenuators in place) lie well above the predicted curve. This apparent discrepancy has been encountered in the spectral analysis of several other flares. It is possible that the presence of a multi-thermal or two-component emission measure spectrum contributes to this discrepancy or that plasma with

a higher iron abundance appears at this time, but instrumental explanations for these anomalous variations are also under investigation.

Since both line features seen in RHESSI spectra are believed to be produced primarily from iron, it should be possible to obtain a measure of the plasma temperature independent of the iron abundance from the flux ratio of the two line features. Caspi et al. (2004) analyzed RHESSI spectral observations for several flares and determined this line ratio as a function of the temperature derived from the continuum. The results for one flare are commpared in Fig. 3 with the Chianti-predicted variation in this line ratio with plasma temperature. There is general agreement between the measured and predicted values suggesting that this is a viable alternative method for determining the plasma temperature. However, there are significant deviations from the predicted values at certain times during the flare. Analyses of other flares also show similar significant deviations during a flare and from flare to flare. These discrepancies may be the result of the multi-temperature nature of the flare plasma, but possible instrumental interpretations are also under investigation to explain these unexpected results.

3.2 Microflares

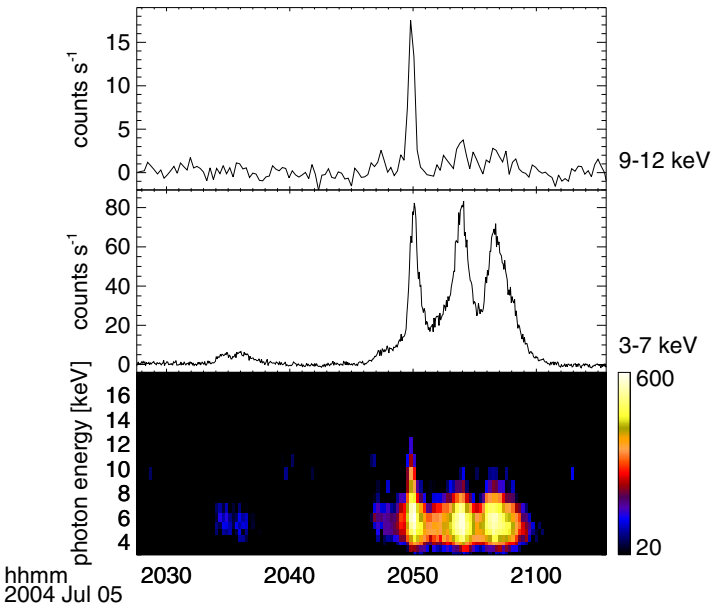

Fig. 4. RHESSI observations of a series of at least 5 microflares in the space of about 30 minutes on July 5, 2004. The top and middle time profiles are for the indicated energy ranges of 9 - 12 and 3 - 7 keV, respectively. The bottom plot is a spectrogram representation of the same data.

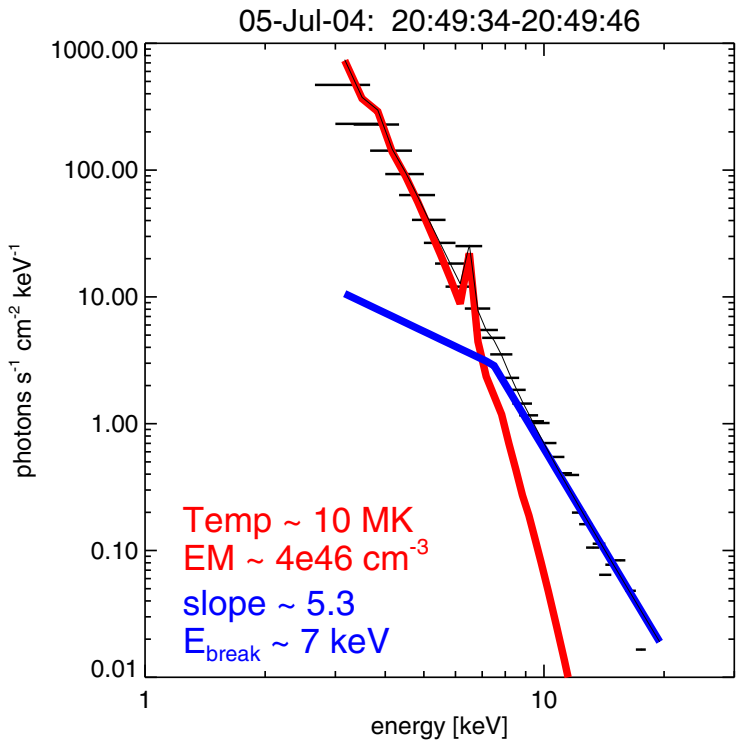

Fig. 5. Fitted spectrum of the hardest microflare shown in Fig. 4 at around 20:49 UT. A thermal (red or dark gray) and non-thermal (power-law) fit (blue or black) is shown. A spectral index γ of 1.7 was assumed below the ∼7 keV break energy. A fit with two thermal components gives a slightly worse, but still acceptable, fit. It gives a high temperature of ∼35 MK for the hotter component with an emission measure about 130 times smaller than that of the cooler component.

Fig. 4 shows an example of RHESSI microflare observations (see also Benz & Grigis 2002, Krucker et al. 2002, Liu et al. 2004, Qiu et al. 2004). Spectral investigations show the existence of a thermal and a non-thermal component (Fig. 5). The power-law fits ($\epsilon^{-\gamma}$) to the non-thermal component of the photon spectrum extend to below 7 keV with values of γ between 5 and 8. They imply a total non-thermal electron energy content of between 10^{26} and 10^{27} ergs (Benz & Grigis 2002, Krucker et al. 2002). Except for the fact that the power-law indices are steeper than those generally found in regular flares, the investigated microflares show characteristics similar to large flares. Since the total energy in non-thermal electrons is very sensitive to the value of the power-law index and the energy cutoff, these observations will give us better estimates of the total energy input into the corona. In earlier work with observations above ∼25 keV, the cutoff energy was often set to 25 keV (e.g., Crosby et al. 1993). For regular flares, the use of 10 keV instead of

25 keV gives energies larger by a factor of ∼10. For the microflares present in this work, the factor is ∼500, since the spectra are steeper and the cutoff energy lower. Hence, the correction for smaller events seems to be larger. This would require renormalization of the flare frequency distribution published by Crosby et al. (1993) and would lead to a re-evaluation of the microflare contribution to coronal heating.

3.3 Evidence for a Current Sheet

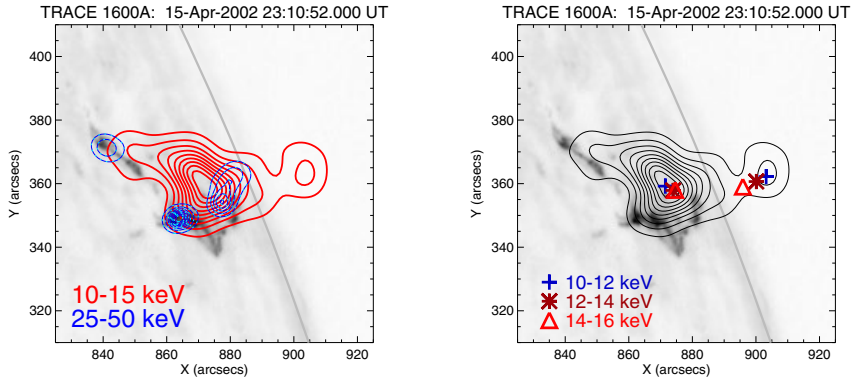

Fig. 6. Left image: TRACE 1600-Å image of the flare that started at 23:07 UT on April 15, 2002, overlaid with RHESSI contours for the indicated energy ranges. Note the loop-top structure in the 10-15 keV source (red or dark gray contours) with a separated source around [905/360] arcsec. HXR emission (dashed blue or gray) is seen from two footpoints ([840/370] and [865/350]), plus a third source around [880/355] that is most probably located in the corona.
Right image: same as the left image but showing only the 10 - 15 keV contours. The centroids of the looptop and coronal sources are shown for the different energies as indicated. Note that the higher energies of the looptop source are at higher altitudes (1 Mm = 1.3 arcsec) whereas the higher energies of the coronal source are at lower altitudes. This suggests that the flare energy must have been released between the two sources. (After Sui & Holman 2003.)

Notwithstanding the observational problems for flare models based on large-scale magnetic reconnection (e.g., Hudson and Khan 1996), several pieces of indirect evidence for such models (e.g., Priest and Forbes 2002) have been reported, mostly using X-ray observations from the Yohkoh Soft X-ray Telescope (SXT) and Hard X-ray Telescope (HXT). Cusp-shaped soft X-ray flare loops were reported by Tsuneta et al. (1992) and Tsuneta (1996), with high-temperature plasma along the field lines mapping to the tip of the cusp. However, Morita et al. (2001) questioned the reality of the cusps in at least one flare. Tsuneta et al. (1992) reported the expected increase of loop height and footpoint separation with time. Masuda et al. (1994) discovered a hard X-ray

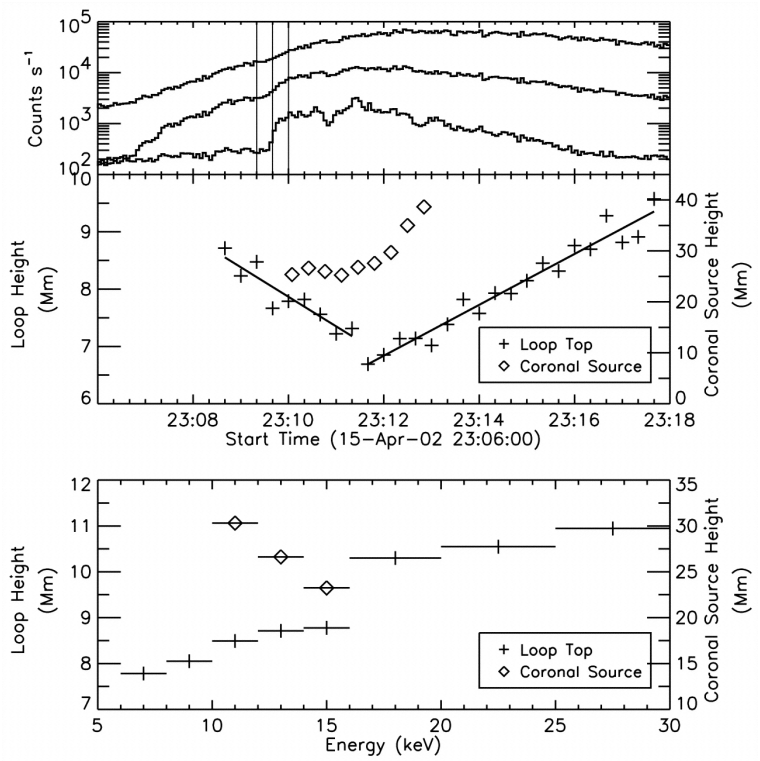

Fig. 7. Top panel: RHESSI light curves in three energy bands (from top to bottom): 3-12, 12-25, and 25-50 keV scaled by factors of 2.0, 0.5, and 1.0, respectively. Middle panel: Time histories of the loop height (obtained from the 10-12 keV images) and the coronal source height (obtained from 10-25 keV images). Bottom panel: Height of the loop and the coronal source at different energies at 23:11:00 UT. After Sui and Holman (2003).

source above the soft X-ray loops. Evidence has been presented for horizontal inflow above the cusp region by Yokoyama et al. (2001), downflow above the loop arcades by McKenzie & Hudson (1999), and an upward-ejected plasmoid above the loops by Shibata et al. (1995) and Ohyama & Shibata (1998).

New evidence for magnetic reconnection has been obtained with RHESSI observations. Sui & Holman (2003) analyzed a series of flares in April 2002, all from the same active region, showing bright flare loops and coronal X-ray sources above them. Such an X-ray source structure is shown in Fig. 6, where RHESSI contours are overlaid on a contemporaneous TRACE image taken during the impulsive phase of one of these flares on 15 April. Both a bright loop and a source above the loop are evident in this image. The projected altitudes of these X-ray sources vs. time and energy are plotted in Fig. 7, along

with the X-ray light curves in different energy bands. Initially, the centroid of the bright loop-top source appeared to move to lower altitudes at about $\sim$9 km s^{-1}. Similar initial decreases in apparent height have been reported for other flares (Sui et al. 2004). The reason for this initial fall is not known or predicted by any of the reconnection models. Sui et al. speculate that it could be the result of the newly reconnected field lines relaxing to a near semicircular state. Alternatively, it could be support for implosion (Hudson 2000).

After the impulsive rise, the upper part of the coronal source separated from the underlying flare loop. Sui and Holman (2003) speculate that this is the result of the initial X-type magnetic configuration evolving into a current sheet with a Y-point at each end (Priest & Forbes 2002). The X-ray bright underlying loops appeared to rise at $\sim$8 km s^{-1} after the HXR emission had peaked. The separated coronal source was stationary at first but then moved out of the RHESSI field of view at $\sim$300 km s^{-1}.

When this result was first presented, the reality of the relatively weak coronal source above the loop top was questioned since it was only $\sim$20% as intense as the looptop source, i.e., close to the current RHESSI dynamic range capability. However, TRACE 195Å difference images recently prepared by Veronig (private communication) for a similar flare on 16 April 2002 show a rapidly moving structure, co-spatial and co-temporal with the RHESSI coronal source, thus dispelling lingering doubts that this relatively weak source might be an artifact of the RHESSI Fourier imaging technique.

The remarkable feature of the loop-top source and the overlying coronal source reported by Sui and Holman (2003) is their oppositely directed temperature gradients as determined from the RHESSI images - the temperature of the underlying loops increased with apparent altitude whereas the temperature of the separated coronal source decreased with altitude. This is illustrated in Fig. 6 (right), where centroid locations are shown for the two sources at different energies during the peak in HXRs. This composite image shows that the highest temperatures are located in the regions where the two sources are closest to one another (Fig. 6 right). This effect can also be seen in the bottom panel of Fig. 7, where the apparent altitudes of the two sources are plotted vs. photon energy. Note the opposite dependence on energy of the looptop and coronal sources. Sui & Holman (2003) interpret this as strong evidence that the energy must have been released between the two sources by magnetic reconnection in a current sheet. This results in the formation of new bright structures both above and below the current sheet. The new structures are hotter than those formed earlier since the latter cool rapidly by both conduction and radiation.

How the newly formed magnetic structures become filled with hot X-ray emitting plasma is not certain. In the classic flare model, the magnetic reconnection accelerates electrons that propagate down the field lines to the footpoints. There, they emit the observed HXRs and heat the chromospheric gas, which moves explosively back up (the so-called chromospheric evaporation),

filling the loop with hot plasma. Feldman (2005) has pointed out significant problems with this scenario and suggests instead that in situ heating of the gas in the current sheet produces the bright loop-top thermal sources. This would also explain the appearance of the hot source above the looptops, which is difficult to account for in the classic chromospheric evaporation model. Clearly, observations of other flares are needed to resolve these issues.

4 Hard X-Rays

At energies above the thermal emissions, the hard X-rays provide the most direct information about the electrons accelerated during the flare. An early flare observed with RHESSI on 20 February 2002 provides a relatively simple example of the information that is available and how it can be interpreted (Krucker and Lin 2002, Aschwanden et al. 2002, Sui et al. 2002). RHESSI images at the HXR peak of this flare are shown in Fig. 8. They are interpreted as showing both thermal emission from a hot loop at low energies and nonthermal emission from footpoints at high energies. Even in this simple case, however, the situation is more complicated since a weak but significant source is seen closer to the limb, particularly in the 16-18 keV image in Fig. 8. Sui et al. (2002) interpreted this as a high altitude source around the top of a larger loop or arcade of loops.

The spatially integrated spectrum of this same flare on 2002 February 20 shown in Fig. 9 provides for a clean separation between the thermal and nonthermal emissions. It supports the view suggested by the images of Fig. 8 that thermal emission dominates below ∼10 keV. The nonthermal spectrum seems to extend down to ∼10 keV. This means that the energy in the accelerated electrons is significantly higher for this event than would have been estimated previously by arbitrarily assuming a lower cutoff energy of 20 or 30 keV. This becomes increasingly important for steep nonthermal spectra and can have major implications in estimating the importance of the accelerated electrons in the overall flare energy budget as discussed below in section 6.

The fitted spectrum shown in Fig. 9 was determined using a forward-folding method starting with a double power-law electron distribution having a low-energy cutoff. The resulting bremsstrahlung photon spectrum was computed assuming thick-target interactions. A thermal spectrum was then added to it and the combination folded through the RHESSI instrument response matrix to give a predicted count-rate spectrum. The parameters of the electron distribution and the thermal spectrum were then modified iteratively to minimize the value of χ^2 relating the predicted and measured count-rate spectra.

Other spectral analysis techniques have been tried to avoid having to make any assumptions about the form of the electron distribution. Kontar et al. (2005) have used an inverse regularization method to analyze RHESSI data for a flare on 26 February 2002. They conclude that a suspected dip in the

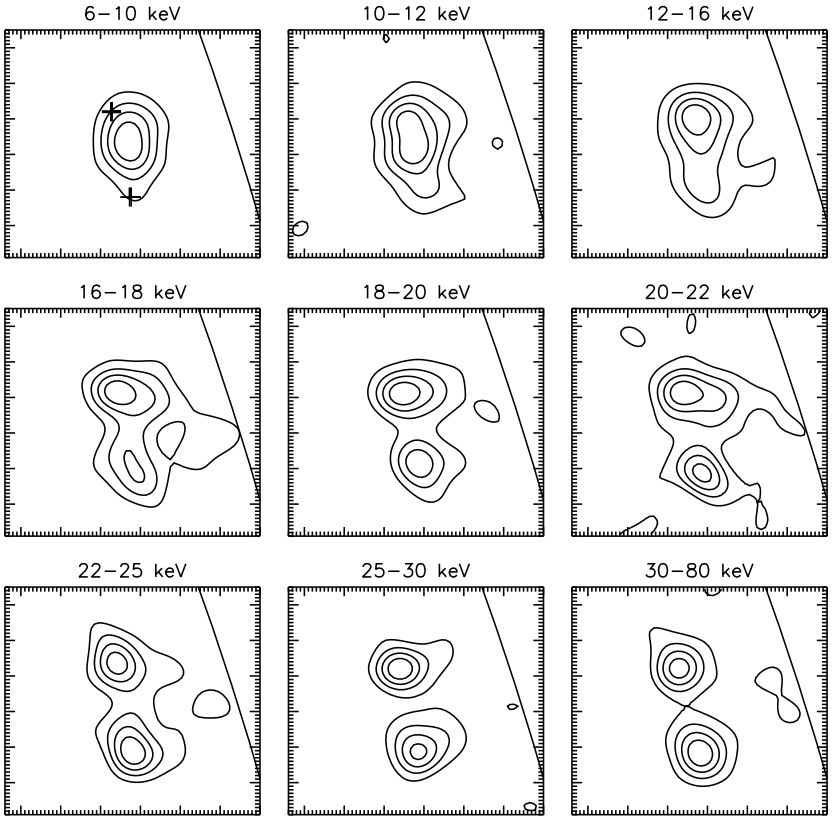

Fig. 8. RHESSI Cleaned images in different energy ranges between 6 and 80 keV for the flare on 20 February 2002 from 11:06:000 to 11:06:39.6 UT. The thermal source can be seen at low energies, below ∼15 keV, between the two footpoint sources that are clearly separated at higher energies. The contour levels are at 20, 40, 60, and 80% of the peak value in each image. The plus signs (+) in the 6 - 10 keV image mark the peaks of the two sources seen at 30 - 80 keV.

spectrum at ∼ 20 keV and a similar dip at ∼55 keV reported by Piana et al. (2003) for the 23 July 2003 flare cannot be confirmed but must, at present, remain a tantalizing mystery.

RHESSI's imaging spectroscopy capability allows us to determine independent spectra for the spatially separated sources. This can be seen from the images in Fig. 8. Sui et al. (2002) showed that the footpoint photon spectra can be fit with a power-law having $\gamma = 3$, whereas the looptop region has $\gamma = 4$. Krucker and Lin (2002) obtain similar values for γ but with a break at about 20 keV early in the flare and softening with time after the peak.

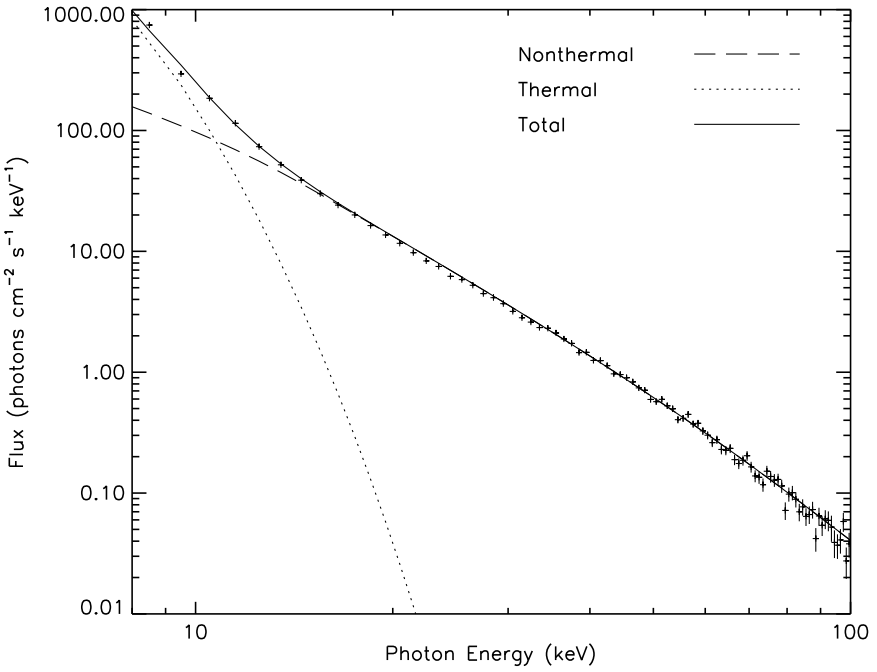

Fig. 9. RHESSI spatially integrated photon spectrum of the flare on 20 February 2002 for a 14-s time interval starting at 11:06:10 UT (after Sui et al. 2002). The indicated thermal and nonthermal curves give the best fit to the count-rate spectrum. The thermal continuum spectrum is for a temperature of 15 MK and an emission measure of 2×10^{48} cm^{-3}. The nonthermal spectrum is the photon spectrum that would be produced by a double power-law electron spectrum assuming thick-target interactions. The spectral index (δ) of the electron spectrum used for the fit is 4.4 below a break energy of 100 keV and 5.5 at higher energies.

Aschwanden et al. (2002) were able to determine the height of the footpoint sources as a function of energy from the small arcsecond differences in the location of the source centroids in different energy bands. They found agreement with the predictions of the thick-target model assuming the very simple Caltech Irreference Chromospheric Model (CICM, Ewell et al. 1993).

The high resolution and statistical accuracy of the energy spectra being measured with RHESSI allow more subtle effects to be investigated beyond the simple thermal and power-law spectra. In particular, the albedo component of the flux significantly modifies the measured spectrum, as pointed out by Brown (1975), Bai and Ramaty (1978) and Alexander and Brown (2002). The extended 'halo' source around more compact HXR sources reported by Schmahl and Hurford (2002a and b) may be interpreted as the albedo component. Other interpretations are still possible, however, such as thin-target or thermal loops, or other unidentified diffuse structures.

A second effect associated with the thick-target interpretation of the HXR emission is the varying ionization along the electron paths (Brown 1973). It is expected that the plasma will be fully ionized in the coronal magnetic loops but that the ionization level will decrease with depth in the chromosphere. The long-range collisional energy losses are reduced as the ionization level falls, resulting in a higher effective HXR bremsstrahlung efficiency. Consequently, the HXR emission at high energies ($\geq$100 keV) is a factor of 2.8 more intense for electrons that penetrate down to the neutral gas target than for lower energy electrons that stop in the fully ionized plasma in the corona. The predicted HXR spectrum from a power-law electron injection spectrum of the form $E^{-\delta}$ (where E is the electron energy) has a power-law index of $\gamma = \delta - 1$ at both low and high energies but $\gamma < \delta - 1$ in between.

As shown in Fig. 9, RHESSI photon spectra often show deviations from a simple power-law in the range from 20 - 100 keV. Such spectral breaks may be associated with an acceleration process that gives corresponding breaks in the electron spectrum. However, Kontar et al. (2002) pointed out that they could be the result of the effects of changes in the ionization level across the transition region, and that the electron spectrum could still be a simple power-law as expected from some acceleration models. Other effects, such as the albedo flux discussed above and various instrumental effects, could also result in breaks in the photon spectrum that are not an indication of breaks in the electron spectrum. Important instrumental effects that remain uncertain are pulse pile up at counting rates above $\sim$10,000 counts per detector (complicated by the image-dependent modulation of the counting rates), uncertainties in the instrument response matrix, and uncertainties in the background that must be subtracted from the measured count-rate spectrum. All of these effects are being actively investigated so that the full potential of the RHESSI observations can be achieved.

4.1 Separation of Thermal and Nonthermal Emission

Conventionally, one separates the HXR spectrum into a thermal and a nonthermal component. This is a most important, but often a very difficult task in the analysis of RHESSI observations. It is critical in determining the relative energies in the thermal plasma and in the accelerated electrons; this will be revisited in section 6 on flare energetics.

Sometimes the separation of thermal and nonthermal emission can be relatively easy, as, for example, when we see hard X-ray emission from two bright sources that can be identified as the footpoints of magnetic loops or arcades. This is the case in the images of the 20 February 2002 flare shown in Fig. 8. Strong evidence that such footpoint emission is nonthermal comes from the simultaneity to within 0.1 s of the peaks from the two footpoints for the flares presented by Sakao (1994) and Sakao et al. (1995) based on Yohkoh HXT observations. Convincing indirect evidence comes from the close association

of HXR footpoint emission with low-temperature emissions such as the white-light continuum (e.g., Metcalf et al., 2001).

One can usually be safe in assuming that a coronal HXR source is thermal but this may not always be true. For example, both Lin et al. (2003) and Veronig and Brown (2004) have argued that coronal HXR sources seen in two different flares were, in fact, nonthermal.

The HXR time history in the impulsive phase is also an indicator of the thermal or nonthermal nature of the sources - the more impulsive emission is thought more likely to be nonthermal. This cannot be demonstrated unambiguously, however, but it is often a useful clue that can support or oppose assumptions made on the basis of other information.

Spectrally, there is often a clear distinction between the steep thermal component at lower energies and the flatter, power-law function at high energies, as shown in Fig. 9. Frequently, however, especially during the early stages of a flare, there is no clear spectral distinction, and a power-law with a single index can fit the data from the lowest energies covered by RHESSI up to the highest energies at which the flare emission is above the instrumental background level. Holman et al. (2003) faced this problem in their analysis of the HXR spectra for the 23 July 2002 gamma-ray line flare. Before the main impulsive rise in HXRs, the count-rate spectrum could be fit equally well above 10 keV with a double power-law electron spectrum alone or with an isothermal component and a double power-law function above an electron energy of 18 keV. Also, it could be fitted with a multi-temperature thermal function over the full energy range. If they assumed that all of the emission above 10 keV was from a nonthermal distribution of high energy electrons, then they arrived at the unlikely conclusion that most of the flare energy was released prior to the major HXR burst. Thus, it seems likely that at least some of the emission may have been from plasma at temperatures as high as several tens of MK.

The separation of thermal and nonthermal emission can be aided by the analysis of the Fe-line features in the spectrum below 10 keV as discussed in section 3.1, since it is safe to assume that the Fe-line emission is from thermal plasma. While it is possible that inner-shell lines (Kα, Kβ) can be generated by impact ionization with high-energy particles, no evidence for such a production process has ever been detected using the various high-resolution crystal spectrometers on SMM, Yohkoh, and Coronas-F (Phillips, private communication; see Emslie et al. (1986) for a possible counter-example). This, then, has consequences for the continuum that must accompany the line emission. The temperature, iron abundance, and line flux that can be obtained from the RHESSI observations of the iron-line feature can be used to constrain the possible thermal continuum, and, hence, allow the nonthermal component to be more accurately estimated in the region of overlap.

4.2 HXR Flares and Escaping Electrons

Some of the electrons accelerated in a flare lose their energy by collisions in the denser, lower solar atmosphere producing the HXR emission seen with RHESSI, while others escape into interplanetary space. Consequently, an interesting comparison can be made between RHESSI flare HXR measurements and the in situ electron measurements made in the vicinity of the Earth. Whether the HXR-producing electrons and the escaping electrons are accelerated by the same mechanism is not known. Combining RHESSI HXR observations with in situ observations of energetic electrons near 1 AU from the WIND spacecraft (Lin et al. 1995) allows a detailed temporal, spatial, and spectral study to be made for the first time. Early results show that events with a close temporal agreement between the HXR and the in-situ detected electrons (taking the time of flight of the escaping electrons into account) show a correlation between the HXR photon spectral index and the electron spectral index observed in-situ (Krucker, Kontar, & Lin 2005) indicating a common acceleration mechanism. Furthermore, the X-ray source structure of these events looks similar, showing hot loops with HXR footpoints plus an additional HXR source separated from the loop by $\sim$15 arcseconds (Fig. 10 left). This source structure can be explained by a simple magnetic reconnection model with newly emerging flux tubes that reconnect with previously open field lines as shown in Fig. 10 (right).

4.3 HXR Footpoints

Solar HXR bremsstrahlung from energetic electrons accelerated in the impulsive phase of a flare is generally observed to be primarily from the footpoints of magnetic loops (see Fig. 8 for an example). The mechanism that accelerates the electrons is still not known but standard 2D magnetic reconnection models predict increasing separation of the footpoints during the flare (e.g., Priest and Forbes 2002) as longer and larger loops are produced. If the reconnection process results in accelerated electrons (Øieroset et al. 2002), the HXR footpoints should show this apparent motion. The motion is "apparent" because it is due to the HXR source shifting to footpoints of neighboring, newly reconnected field lines. Hence, the speed of footpoint separation reflects the rate of magnetic reconnection, and should be roughly proportional to the total HXR emission from the footpoints. Sakao, Kosugi, & Masuda (1998) analyzed footpoint motions in 14 flares observed by Yohkoh HXT, but did not find a clear correlation between the footpoint separation speed and the HXR flux. Recently, however, Qiu et al. (2002) found some correlation between the source motion seen in Hα and the HXR flux during the main peak of a flare, but not before or after. Fletcher & Hudson (2002) carried out similar analysis of footpoint motion using early RHESSI observations of several GOES M-class flares. They found systematic, but more complex footpoint motions than a simple flare model would predict.

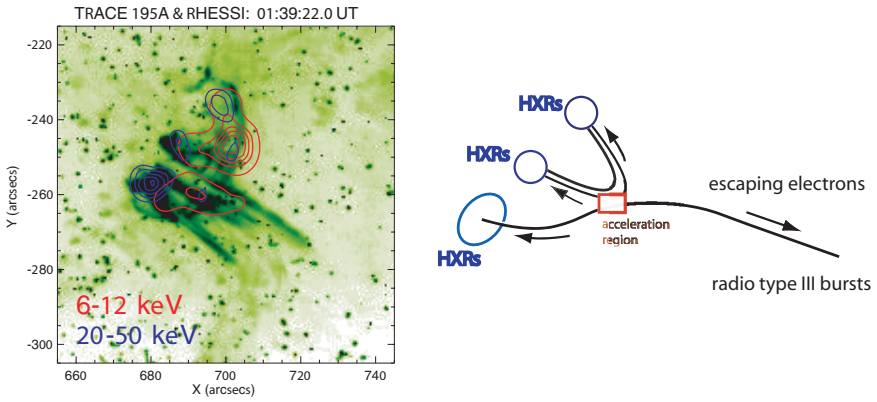

Fig. 10. EUV and X-ray sources of a flare that released energetic electrons into interplanetary space that were later observed near the Earth.
Left figure: RHESSI contours at 6 - 12 keV (red or dark gray: thermal emission) and 20 - 50 keV (blue or black: non-thermal emission) overlaid on a TRACE 195Å EUV image (dark region corresponds to enhanced emission). Located at around [700,-245] arcsec, the X-ray emission outlines a loop with two presumably nonthermal footpoints . The strongest footpoint source however, is slightly to the southeast [683,-257] and shows a surprisingly lower intensity thermal source.
Right figure: Suggested magnetic field configuration showing magnetic reconnection between open and closed field lines inside the red or dark gray box marked as the "acceleration region" where downward moving electrons produce the HXR sources and upward moving electrons escape into interplanetary space.

Footpoint motion can be best studied in the largest events that show intense HXR emission lasting for many minutes. Krucker, Hurford, & Lin (2003) analyzed HXR footpoint motions in the July 23, 2002 flare (GOES X4.8). As can be seen in Fig. 11, at least three HXR sources above 30 keV can be identified during the impulsive phase with footpoints of coronal magnetic loops in an arcade. On the northern ribbon of this arcade, a source (f1) is seen that moves systematically along the ribbon for more than 10 minutes. On the southern ribbon, at least two sources (f2 and f3) are seen that do not seem to move systematically for longer than 30 s, with different sources dominating at different times. The northern source motions are fast during times of strong HXR flux, but almost absent during periods with low HXR emission. This is consistent with magnetic reconnection if a higher rate of reconnection of field lines (resulting in a higher footpoint speed) produces more energetic electrons per unit time and therefore more HXR emission. The absence of footpoint motion in one ribbon is inconsistent with simple reconnection models.

An additional correlation predicted from the simple theoretical reconnection model is between the footpoint motion and the rate of energy deposited by the energetic electrons into the footpoints. The idea is that the higher

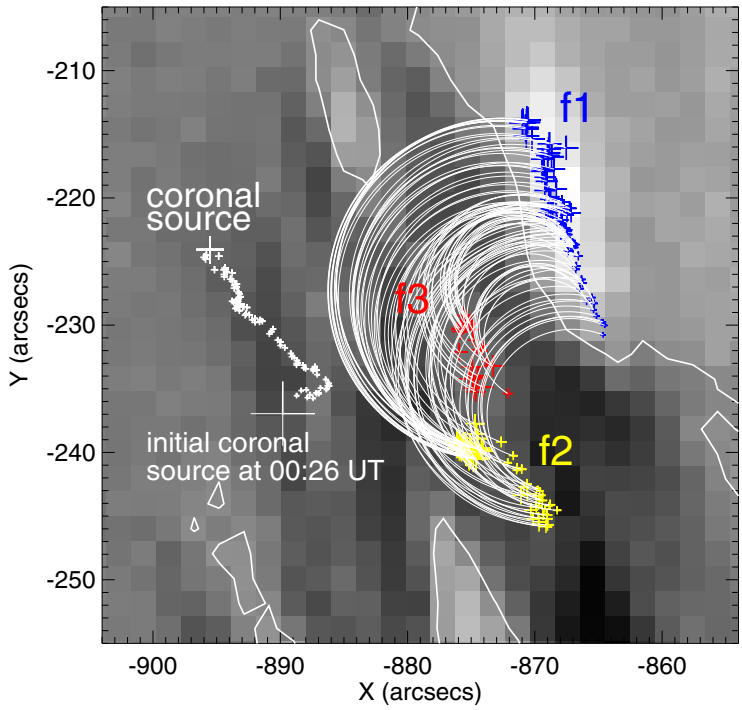

Fig. 11. Temporal evolution of the HXR sources seen with RHESSI during the flare on 23 July 2002. The motions of footpoints f1 (black crosses), f2 (white crosses), and f3 at 30–80 keV and the coronal source (white crosses) at 18–25 keV are indicated by the increasing size of the symbols to represent times from 00:26:35 to 00:39:07 UT. The centroid positions of the different sources are shown every 8 s for the footpoints and every 26 s for the coronal source. The semicircles connect simultaneously brightening footpoints. Note that the coronal source seems to be at a higher altitude than the tops of these ad-hoc semicircles. The grey-scale image is an MDI magnetogram in which the apparent neutral line is shown in white and the extreme line-of-sight values of the magnetic field are ±600 G (from Krucker, Hurford, & Lin 2003).

the reconnection rate, the more electrons are accelerated and the faster the footpoints move apart. The rate of energy deposition into the footpoints can be readily determined from the RHESSI imaging spectroscopy observations of the 23 July 2002 event assuming thick-target interactions. Combining this with the footpoint velocities derived from Fig. 11 gives a rough correlation as expected. Since this flare was close to the limb, the magnetic field strength could not be well determined in the footpoints, but assuming a constant value of 1000 G, we get the reconnection rates varying between $\sim$1 and 5 $\times$ 10^{18} Mx s^{-1} . These results are consistent with a model in which a higher rate of

magnetic reconnection makes the footpoints move faster and also accelerates more electrons and deposits more energy at the footpoints.

5 Gamma Rays

The acceleration of ions to high energies in large solar flares has been established by the detection of nuclear gamma-ray line emission (e.g., Chupp 1990). When energetic ions collide with the solar atmosphere, they produce excited nuclei that emit prompt nuclear de-excitation lines, as well as secondary neutrons and positrons that result in the delayed 2.223 MeV neutron-capture line and the 511 keV positron-annihilation line (Ramaty & Murphy 1987). Because of Doppler broadening, the line widths are dependent on the temperature or the velocity distribution of the emitting particles. High-energy protons interacting with the heavy ions of the ambient atmosphere produce relatively narrow gamma-ray lines characteristic of the different elements. High-energy heavier ions interacting with ambient protons, on the other hand, produce much broader lines because of the high velocities of the emitting ions. Also, accelerated α particles give detectable line features below 500 keV when they interact with ambient helium nuclei, the so-called α-α interactions. Spectral observations of all of these features, both the narrow and broad lines, provide information on the energy spectrum and composition of the accelerated ions and on the composition of the ambient target atmosphere (e.g., Chupp 1984; Share & Murphy 1995). All of these gamma-ray emissions are evident in the RHESSI spectrum shown in Fig. 12 for the X17 flare on 28 October 2003. The best-fit templates of the expected features are also shown for clarity. For the first time, RHESSI has the energy resolution necessary to resolve all of these gamma-ray lines, except for the intrinsically narrow 2.223 MeV line, and to determine the detailed line shapes expected from Doppler-shifts and the different possible velocity distributions. In addition, RHESSI provides the first spatial information on the gamma-ray sources, the only direct indication of the spatial properties of accelerated ions near the Sun.

5.1 The 511 keV Positron-Annihilation Line

Positrons are produced in solar flares from the decay of both radioactive nuclei and pions that themselves are the result of interactions of the flare accelerated ions in the solar atmosphere. The production of observable gamma-rays from the positrons is not a straightforward process. A fortunate consequence of the complications is that much unique information can be obtained about the ambient medium through which the positrons pass from production to annihilation. Before the positrons can interact with the ambient thermal electrons, they must slow down by collisions until they have similar velocities. Then, a positron can either annihilate directly with a bound or a free electron to produce two 511-keV photons traveling in opposite directions, or it can combine

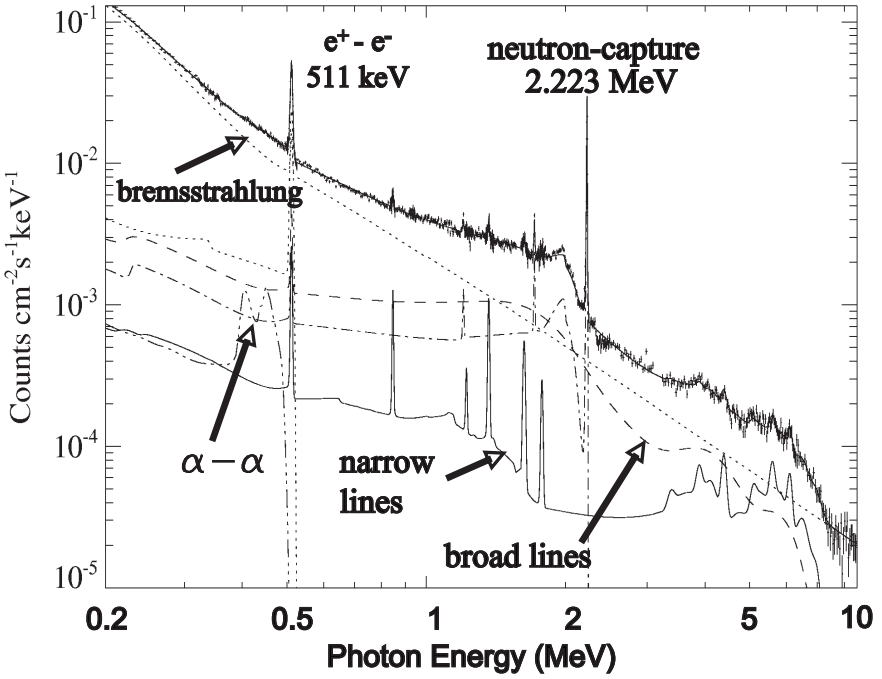

Fig. 12. RHESSI count-rate spectrum recorded during the X17 flare on 28 October 2003 from 11:06:20 to 11:10:04 UT. Clearly evident in this spectrum is the prominent neutron-capture line at 2.223 MeV, the positron annihilation line at 511 keV, numerous other narrow lines from accelerated protons, broad lines from accelerated heavy ions, and the features below 500 keV from α-α interactions. Underlying the line features is the bremsstrahlung continuum from accelerated electrons. Fitted templates of the expected spectra for the different components are also indicated. (After Share et al. 2005.)

with a bound or free electron to produce a hydrogen-like positronium 'atom' consisting of the positron and an electron in orbit around one another. After a while, the positronium decays in one of two ways depending on the relative spins of the two particles. If the spins are antiparallel (the singlet state), then the two particles annihilate, again with the production of two oppositely directed 511-keV photons. If the spins are parallel (the triplet state), then three photons are produced, all with energies below 511 keV. This latter case is observable as a continuum below the 511-keV line. The continuum-to-line ratio is called the $3\gamma/2\gamma$ ratio and its determination is an important goal of the spectral analysis of RHESSI data for individual flares.

Further complications arise because the positronium can be formed either by thermal charge-exchange when essentially at rest, or by charge-exchange in

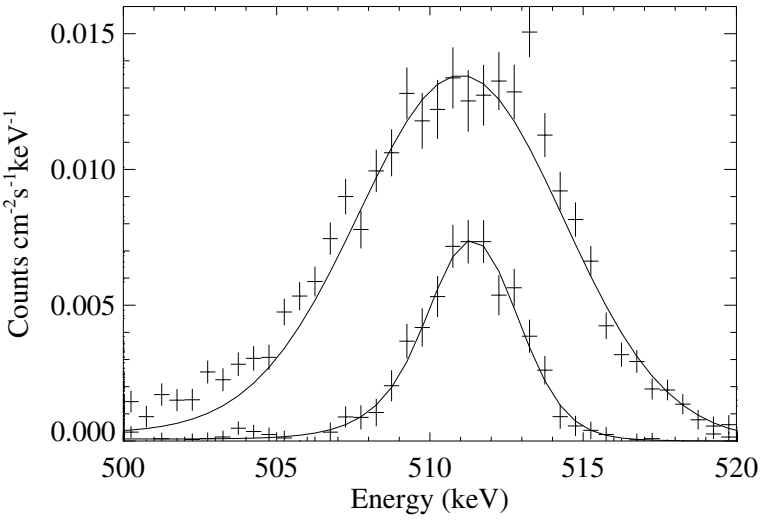

Fig. 13. Count spectra of the 511-keV positron-annihilation line, after subtracting bremsstrahlung, nuclear, and induced 511-keV line contributions, for two different times during the 28 October, 2003, X17 flare. The broad line was obtained between 11:06 and 11:16 UT, and the narrow line between 11:18 and 11:30 UT. The solid curve in each case is the best-fitting model that includes a Gaussian line centered at 511-keV and the positronium continuum at lower energies. (After Share et al. 2004.)

flight. In the first case, the subsequent decay results in a very narrow 511-keV line ($\sim$1.5 keV FWHM). In the second case, the resulting 511-keV line can be Doppler broadened to $\sim$7.5 keV FWHM, easily measurable with RHESSI. At densities above $\sim 10^{13}\,\mathrm{cm}^{-3}$, the 3γ continuum intensity is reduced as a result of collisions that cause transitions from the triplet to the singlet state and the breakup of the positronium, thus affecting the $3\gamma/2\gamma$ ratio.

Although the positron story is complicated, all the processes are well understood. Through careful modeling, the measured 511-keV line shape, the $3\gamma/2\gamma$ ratio, and the time history can provide information on the temperature, density, composition, and ionization state of the ambient medium in which the positrons slow down, form positronium, and annihilate. In this sense, then, the positrons act as a thermometer, a barometer, and an ionization gauge for the ambient solar atmosphere.

RHESSI has now observed at least four flares with sufficient intensity to provide useful diagnostics from the positron-electron annihilation line. The first flare with high-resolution spectral observations of this line occurred on 2002 July 23 (Share et al. 2003a). In that case, the line had a Gaussian width of 8.1 $\pm$ 1.1 keV (FWHM). Two interpretations of this width are possible: either the annihilations took place in a medium with temperatures as high as

$\sim (4-7) \times 10^5$ K or the positronium formation took place by charge exchange in flight at temperatures near 6000 K.

Better statistics were obtained for the X17 flare that started at 09:51 UT on 28 October 2003 (Share et al. 2004). The line profile is shown in Fig. 13 for two different times during the flare. Early in the flare, the annihilation line was broadened to 8 ± 1 keV(FWHM), suggesting temperatures of $> 2 \times 10^5$ K if thermal. Later during the flare, at a time when observations at other wavelengths show that nothing unusual appears to be happening, the line becomes much narrower ($\sim$1 keV) on time scales of a few minutes, suggesting temperatures of less than or $\sim 1 \times 10^4$ K and high ionization levels. In fact, the line became the narrowest that the RHESSI spectrometer has ever measured, in space or on the ground. In Fig. 13, the change in the width of the 511-keV line is evident suggesting a dramatic reduction in temperature of the annihilation region. However, this sudden narrowing poses serious problems for a thermal interpretation. What heats the chromospheric material with densities between 10^{12} and 10^{14} cm^{-3} to such high temperatures and why does it cool so suddenly with no other obvious manifestation?

5.2 Nuclear De-excitation Lines

RHESSI has obtained the first high-resolution measurements of nuclear de-excitation lines produced by energetic ions accelerated in solar flares (Smith et al. 2003). Narrow lines from high-energy proton interactions with ambient neon, magnesium, silicon, iron, carbon, and oxygen, resolved for the first time, are shown in Fig. 14 for the flare of 2002 July 23 at a heliocentric angle of $\sim 73°$. The deviation of the lines from their rest-frame energy and the measured line widths indicate Doppler redshifts of 0.1 - 0.8% and line broadening of 0.1 - 2.1% (FWHM). These values generally decrease with the atomic mass of the emitting nucleus, as expected, since heavier nuclei will recoil less from a collision with a fast proton or α particle. The measured redshifts for this flare are larger than expected for a model of an interacting ion distribution isotropic in the downward hemisphere in a radial magnetic field. To explain these observations, either the ions are traveling along a magnetic loop inclined towards the Earth at $\sim 40°$ to the radial direction, or the ions are highly beamed. Bulk downward motion of the plasma in which the accelerated ions interact can be ruled out (Smith et al. 2003).

5.3 The 2.223 MeV Neutron-Capture Line

Spectroscopy

The production of the intrinsically narrow gamma-ray line at 2.223 MeV, while not as complicated as that of the positron annihilation line, is also subject to various effects that make analysis difficult but potentially very informative. High-energy neutrons are the products of interactions of the accelerated ions

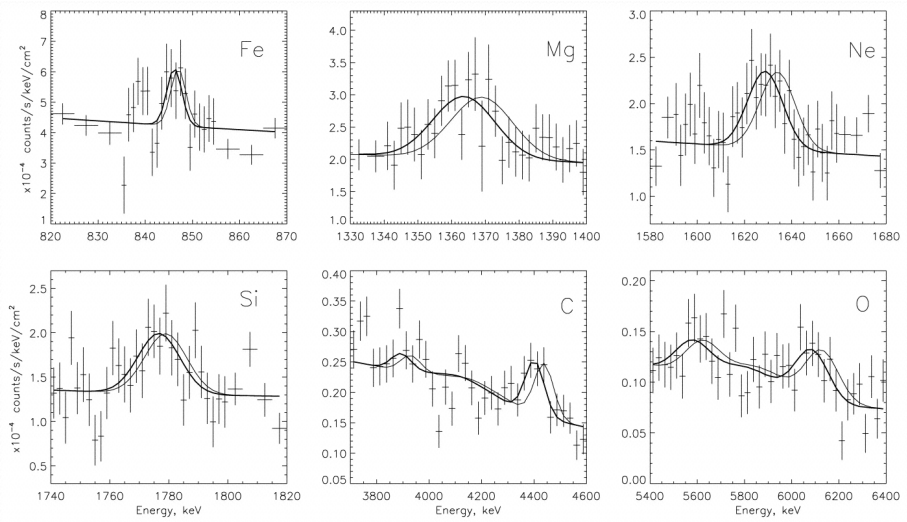

Fig. 14. RHESSI background-subtracted count spectra from 00:27:20 to 00:43:20 UT on 2002 July 23. Each panel is labeled with the element primarily responsible for the line shown. The carbon and oxygen lines also show the secondary peak from the escape of a 511 keV positron-annihilation photon, which also contains information on the line shape. The thick curve shown in each panel is the Gaussian fit from Table 1 plus the underlying bremsstrahlung continuum and broad lines (see text), convolved with the instrument response. The thinner line is the same fit forced to zero redshift for comparison. The error bars are $\pm 1\sigma$ from Poisson statistics. (From Smith et al. 2003.)

with the ambient solar atmosphere. Before they can be captured by ambient thermal hydrogen atoms, however, they must have similar velocities. Consequently, there is a delay while they lose their energy through collisions. Since the neutrons are not constrained by the magnetic fields and can travel relatively long distances, they can penetrate down to photospheric levels before becoming thermalized. After a minute or two, they are captured by hydrogen to form deuterium with the immediate release of a 2.223 MeV gamma-ray carrying the excess binding energy. The line is intrinsically only $\sim$0.1 keV wide since the deuterium is essentially at rest when it is formed.

The first flare observed by RHESSI to show 2.223-MeV line emission occurred on 23 July 2002. The measured FWHM line width was $\sim$4 keV, as expected from the germanium spectral resolution at that energy. The intensity of the line was such that its time history could be determined for a period of about 20 minutes with integration times of 20 s. Murphy et al. (2003) have compared the measured time histories with the predictions of a comprehensive model for particle transport in a magnetic loop that includes Coulomb collisional losses, magnetic mirroring, and pitch-angle scattering. The effects

of neutron capture by ^{3}He and the angular distribution of the accelerated ions that produce the neutrons are also factors that affect the time history. The neutron production rate was assumed to be proportional to the observed flux of 4-to-7.6 MeV gamma-rays produced primarily from nuclear de-excitation of carbon and oxygen. The predicted and measured time histories of the 2.223 MeV line are shown in Fig. 15. Here, the free parameters are the power-law spectral index (s) of the accelerated ions (taken to be 4.5), the mean free path (λ) to isotropize the particle distribution through pitch-angle scattering (taken to be $\lambda = 2000$ times the loop half length, i.e., moderate pitch-angle scattering), and the ^{3}He/H ratio (taken as 7×10^{-5}). The agreement with the observations is remarkable and shows that the accelerated particles must have suffered moderate pitch-angle scattering during their transport through the coronal part of the loop. The derived ^{3}He/H ratio could be better constrained for a flare with stronger nuclear de-excitation line fluxes. Similar analysis is being carried out for the intense flares that occurred during the three week period in October and November 2003, when RHESSI observed and imaged three further gamma-ray line flares.

Imaging

The highest sensitivity for gamma-ray imaging can be achieved by using the 2.223 MeV neutron-capture line. This is because of relatively good statistics and the intrinsically narrow line width, which minimizes the bremsstrahlung continuum contribution and the non-solar background that must be included compared to the broader lines. Hurford et al. (2003) reported a single source structure at this energy for the flare on July 23, 2002, the first gamma-ray-line flare observed by RHESSI. The source was unresolved at the instrumental resolution of 35"; a diffuse source of greater extent than this was excluded by the observations. Surprisingly, the 2.2-MeV source centroid was displaced by 20±6" from the centroid of the HXR sources. The series of very large flares occurring in October/November 2003 confirmed this finding (Hurford et al. 2005). For the event with the best statistics, on October 28, 2003, the 2.2 MeV image in Fig. 16 shows two sources similar to the HXR footpoint sources separated by ∼70 arcsec. However, both the gamma-ray sources appear to be displaced from the corresponding HXR source by ∼15".

The displacement of the gamma-ray and HXR sources suggests that energetic electrons and ions lose their energy at different places in the solar atmosphere. This could be because the electrons and ions are accelerated at different locations or because of different transport effects from a possibly common acceleration site. Emslie et al. (2004) noted that a stochastic acceleration model based on cascading MHD turbulence proposed by Miller (2000) predicts that ion acceleration takes place in the vicinity of large loops or where the Alfven speed is low, while the electron acceleration originates in shorter loops or where the Alfven speed is high. Ion acceleration in long loops and electron acceleration in short loops would explain the different source loca-

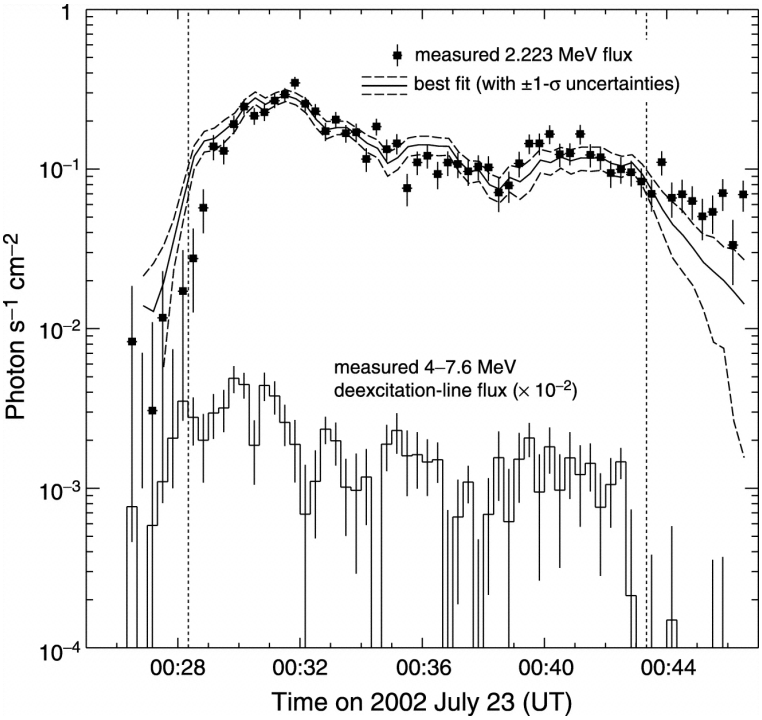

Fig. 15. Measured time history of the 2.223 MeV neutron-capture line compared with the best-fitting predicted line fluxes for s = 4.5 (obtained with $\lambda = 2000$ and ^{3}He/H = 7 /*times* 10^{-5}). The dotted lines indicate the time interval over which the model was calculated (00:28:20 to 00:43:20 UT). The 4-to-7.6 MeV de-excitation line fluxes are also shown, reduced by a factor of 100 for clarity. (After Murphy et al. 2003.)

tions seen in the 23 July flare. However, the October 28, 2003 observations showed similar separations between the two sources seen in HXRs and between the two seen in the 2.2 MeV emission (Fig. 16) suggesting acceleration in similar sized loops. The alternate explanation that electrons are accelerated in regions with high Alfven speeds and ions in regions with low Alfven speeds could apply in both cases.

It is noteworthy that the brightest EUV emission, as indicated by the origin of the TRACE diffraction pattern seen in (Fig. 16), comes from the same location as one of the two HXR footpoints, rather than from one of the gamma-ray sources. Does this indicate that there is more energy in the accelerated electrons than in the ions? Another possible explanation is that the ions will penetrate more deeply into the chromosphere than the electrons and consequently the heated plasma will be cooler and emit preferentially in the UV rather than in the TRACE 195Å passband. It is unlikely that the

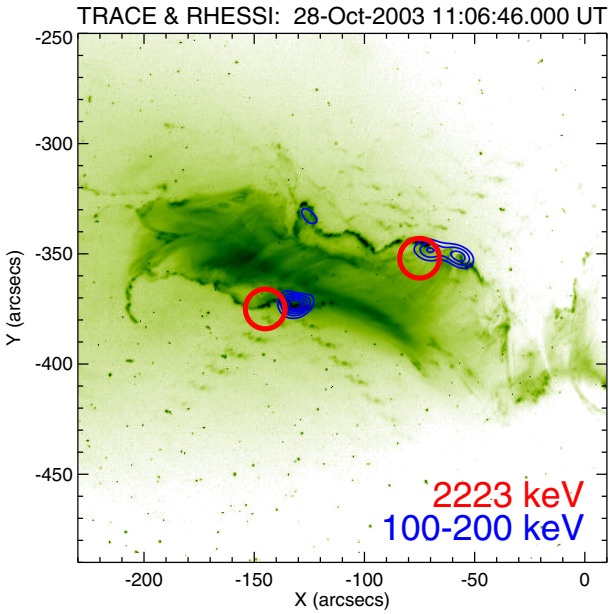

Fig. 16. Imaging of the 2.223 MeV neutron-capture line and the HXR electron bremsstrahlung of the flare on October 28, 2003. The red or gray circles show the locations of the event-averaged centroid positions of the 2.223 MeV emission with 1σ uncertainties; the blue or black lines are the 30, 50, and 90% contours of the 100 - 200 keV electron bremsstrahlung sources at around 11:06:46UT. The underlying EUV image is from TRACE at 195Å with offset corrections applied. The gamma-ray and HXR sources are all located on the EUV flare ribbons seen with TRACE.

different locations of the X-ray and gamma-ray sources is the result of the distance travelled by the neutrons from their point of origin where the bulk of the accelerated ions interact to the place where they become thermalized; this separation is estimated to be only ∼500 km.

6 Flare/CME Energetics

With RHESSI X-ray and gamma-ray observations covering such a broad energy range, it is possible to determine the flare energy distribution with greater precision than previously possible. The energy in the hottest plasmas, the accelerated electrons, and the ions can all be estimated from RHESSI observations with better than the order-of-magnitude accuracy that has previously been possible. Saint-Hilaire and Benz (2002) obtained an energy budget for a flare on 26 February 2002 using RHESSI and TRACE observations. They

found that the energy in the nonthermal electrons producing the HXRs was more than an order of magnitude greater than the thermal and radiated energy in the flare kernel plus the kinetic energy of the jet seen with TRACE. This rather surprising result is consistent with similar conclusions reported by Dennis et al. (2003) based on earlier SMM observations and analysis of the RHESSI observations of the 20 February 2002 flare shown in figures 8 and 9. Saint-Hilaire and Benz (2005) have recently reported on the analysis of RHESSI observations for 9 medium-sized flares, and find that the thermal and nonthermal energies are of the same magnitude.

By combining the RHESSI spectral results with flare observations at other wavelengths, a differential emission measure analysis is being pursued using the Markov-Chain Monte Carlo (MCMC) method described by Lin et al. (2004). This will allow the energetic contributions of the lower temperature gas to be estimated and hence, to determine if it provides a significant contribution to the thermal energy of a flare.

Emslie at al. (2004) report on the first attempt to obtain comprehensive energy budgets for two X-class flares and the associated CMEs, one on 21 April 2002 and the second on 23 July 2002. In addition to the RHESSI flare data, the energetics of the associated CMEs were determined from the SOHO/LASCO observations, and the energy in high-energy particles in space was estimated from the in situ measurements with instruments on ACE, SOHO, and Wind. Unfortunately, the uncertainties on all the different components of the energy are large. The major limitations are that the quoted energies obtained from the RHESSI X-ray and gamma-ray observations are all lower limits. Although reducing the filling factor from the assumed value of $f = 1$ to a possible value as low as 10^{-4} reduces the energy estimate by $\sqrt{f}$, the thermal energy is probably a lower limit because of the underestimate of the radiative and conductive cooling losses. The energy in electrons is a lower limit because of uncertainties in the low-energy cutoff to the electron spectrum. The energy in accelerated ions is a lower limit for the 2002 July 23 flare because of the unknown contribution from ions below a few MeV. (No gamma-ray lines were seen during the 2002 April 21 flare.)

Despite these limitations, Emslie et al. (2004) drew the following tentative conclusions from the results:

1. For the 23 July 2002 flare, the energy in accelerated electrons is comparable to the energy in accelerated ions, in agreement with the conclusion reached by Ramaty et al. (1995) based on SMM results for 19 flares.
2. The CME energy dominates over the combined flare energies in both events.
3. The CME energy is a substantial fraction ($\sim$30%) of the available magnetic energy in both events.

However, conclusion (2) was based on the assumption that the radiant energy from each of the two flares under study was only a factor of two greater than the peak energy in the thermal X-ray emitting plasma. This is contrary

to the factor of ∼5 - 20 obtained from the estimate based on the relationship between the soft X-ray (L_{SXR}) and total (L_{total}) luminosities given by Hudson (1991) and corrected by Shimizu (1995), i.e. $L_{SXR}/L_{total} = 2/30$. This relationship for the 21 April 2002 flare gives a total radiant energy of $10^{31.7}$ ergs. This must be compared to the Emslie et al. values for the available magnetic energy of $10^{32.3\pm\ 0.3}$ ergs, the peak energy in the thermal plasma of $10^{31.1}$ ergs, and radiative losses of $10^{31.3}$ ergs. If the higher value of the radiant energy is accepted, then the flare and CME energies are comparable both to one another and to the available magnetic energy. Clearly, given the order-of-magnitude uncertainties in the flare energies, the energetic dominance of the flare or the CME has not been established by the current estimates for these events. The recent measurement of the total luminosity of the X28 flare on 2003 November 5 (Woods et al. 2004) should provide an accurate normalization of the L_{SXR}/L_{total} ratio for that event.

7 Conclusions

We have tried to provide a representative sampling of the science results from RHESSI solar X-ray and gamma-ray observations. We have not attempted to summarize all of the over 180 RHESSI-related papers that have already been published according to the compilation maintained by Aschwanden at

http://www.lmsal.com/∼aschwand/publications/hessi.html.

Many of the early results were as expected based on previous observations but some have been particularly surprising. Perhaps the most surprising is the apparent displacement between the source of the neutron-capture gamma-ray line and the source of bremsstrahlung X-rays suggesting differences in the acceleration and/or transport of the energetic ions and electrons. The measured gamma-ray line redshifts were expected but their higher than predicted magnitude suggests that the energetic ions were highly beamed or that they traveled along a highly inclined magnetic loop. The intensity of the 511-keV positron annihilation line shows that ∼1 kg of antimatter was produced in the 23 July flare, but how can we interpret the initial heating of the target chromospheric material to such high temperatures that is apparently required by the measurements of the line width. Perhaps a more difficult question is, how does the target material cool so suddenly?

In the hard X-ray domain, RHESSI's high energy resolution has allowed for the most convincing separation to date of the thermal and nonthermal components of the emission. In some cases, the nonthermal spectrum extends down to as low as 10 keV, thus increasing our estimates of the nonthermal energy based on a 25-keV cutoff energy by an order of magnitude or more for average events and by a factor of ∼500 for microflares. The flare energy budget calculations have been aided by RHESSI observations in this way but the energy estimates for the different components are still bedeviled by unknown filling factors and cooling terms. At higher HXR energies, the interest has

been on the downward break in the hard X-ray spectrum often seen between ∼20 and ∼100 keV, suggesting that the electron acceleration process must produce a corresponding break in the electron spectrum. The significance of this for acceleration models has not yet been fully explored.

In its lowest energy domain, RHESSI has provided many interesting observations, thanks to its great sensitivity and sufficient energy resolution to measure the very steep spectra and detect the Fe-line features, even in the more intense flares. The most remarkable result is perhaps the evidence of magnetic reconnection in a current sheet above the flare loops based on the observation of an above-the-looptop source that had a temperature gradient with altitude opposite to that of the underlying loop source. The initial apparent downward motion of this coronal source observed in several flares was a surprise.

Clearly, RHESSI observations are fulfilling the objectives of helping to understand energy release and particle acceleration in solar flares. Much remains to be done in analyzing the many flare observations already made. The instrument is still fully operational and continues to make new flare observations, even as we move towards solar minimum. RHESSI has no consumables, meaning that, barring some unforseen failure of a critical function, it can continue to operate until it re-enters the atmosphere. This will not be, at the earliest, until the rise in solar activity again heats and expands the outer atmosphere. Thus, it is hoped that RHESSI can be kept operating well into the next maximum of activity, allowing it to continue making unique observations of flares over a complete solar cycle and detecting more of the very rare gamma-ray-line events that are so revealing.

Acknowledgments

RHESSI is named for the late Reuven Ramaty, a co-investigator at Goddard Space Flight Center and a pioneer in the fields of solar physics, gamma-ray astronomy, nuclear astrophysics, and cosmic rays.

We thank the whole RHESSI team - without their dedicated effort, none of this would have been possible. We are also indebted to the innumerable scientists around the world who have participated in the analysis and scientific interpretation of the observations. Thanks for sharing your work so freely and for participating in the numerous workshops that have contributed so wonderfully to the cross-fertilization of information and ideas.

For reviewing early drafts of the paper, we thank Leah Haga, Gordon Holman, Gordon Hurford, Ron Murphy, Kenneth Phillips, Gerry Share, and Linhui Sui. We thank Amir Caspi for Fig. 3, Gerry Share for Fig. 12, and Gordon Hurford for Fig. 16, all of which were made available to us prior to publication. We thank the referee, Gordon Emslie, for doing such a careful job that significantly improved the accuracy and readability of the paper.

Finally, we thank Ludwig Klein for inviting us to the CESRA Workshop on the Isle of Skye in Scotland and for insisting so strenuously and persistently that we write this paper.

HSH and SK are supported in part by NASA contract NAS5-98033.

References

1. Alexander, R. C. and Brown, J. C. 2002, Solar Physics, 210, 407-418.
2. Bai, T. and Ramaty, R. 1978, ApJ., 219, 705.
3. Benz, A.O., Grigis, P.C., 2002, Sol. Phys., 210, 431.
4. Brown, J. C., van Beek, H. F., and McClymont, A. N. 1975, A&A, 41, 395-402.
5. Brown, J. C. 1973, Solar Physics, 28, 151.
6. Caspi, A., Krucker, S., and Lin, R. P. 2004, COSPAR presentation, COSPAR04-A-03582 E2.3-0013-04.
7. Chupp, E. L. 1984, ARA&A, 22, 359.
8. Chupp, E. L. 1990, Phys. Scr., T18, 15.
9. Crosby, N.B., Aschwanden, M.J., Dennis, B.R., 1993, Sol. Phys., 143, 275.
10. Dennis, B. R., Veronig, A., Schwartz, R. A., Sui, L., Tolbert, A. K., and Zarro, D. M. 2003, Advances in Space Research, v. 32, no. 12, pp. 2459 - 2464.
11. Dennis, B. R., Phillips, K.J.H., Sylwester, J., Sylwester, B., Schwartz, R.A., and Tolbert, A.K., Advances in Space Research, 2005, in press.
12. Dere, K. P., Landi, E., Mason, H. E., Monsignori Fossi, B. C., & Young, P. R., CHIANTI – An Atomic Database for Emission Lines, 1997, *A&AS*, 125, 149.
13. Emslie, A. G., Phillips, K. J. H., and Dennis, B. R. 1986, Slar Physics, 103, 89-102.
14. Emslie, A. G., Kontar, E.P., Krucker, S, Lin, R.P., 2003, ApJL, 595, L107.
15. Emslie, A. G., 2003, ApJL, 595, L119 - L121.
16. Emslie, A. G., Kucharek, H., Dennis, B. R., Gopalswamy, N., Holman, G. D., Share, G. H., Voulidas, A., Forbes, T. G., Gallagher, P. T., Mason, G. M., Metcalf, T. R., Mewaldt, R. A., Murphy, R. J., Schwartz, R. A., and Zurbuchen, T. H., 2004, J. Geophys. Res., 109, A10104.
17. Emslie, A. G.; Miller, J.A.; Brown, J.C., 2004, ApJL, 602, L69.
18. Ewell, M. W. (jr.), Zirin, H., Jenson, J. B., and Bastian, T. S. 1993, ApJ, 403, 426 - 433.
19. Feldman, U., 2005, in preparation.
20. Fletcher, L., Hudson, H.S., 2002, Solar Physics, 210, 307.
21. Hudson, H. S. 2000, ApJ, 531, L75 - L77.
22. Hurford, G. J., Schwartz, R. A., Krucker, S., Lin, R. P., Smith, D. M., Vilmer, N. 2003, ApJL, 595, L77.
23. Hurford, G. J. et al. 2005, in preparation.
24. Kontar, E. P., Brown, J. C., and McArthur, G. K. 2002, Solar Physics, 210, 419-429.
25. Kontar, E. P., Emslie, A. E., Piana, M., Massone, A. M., Brown, J. C. 2005, Solar Physics, submitted.
26. Krucker, S., Christe, S., Lin, R.P., Hurford, G.J., Schwartz, R.A., 2002, Sol. Phys., 210, 445.
27. Krucker, S. and Lin, R. P. 2002, Solar Physics, 210, 229 - 243.
28. Krucker, S., Hurford, G.J., Lin, R.P., 2003, ApJL, 595, L103.
29. Krucker, S., Kontar, E., Lin, R.P., 2005 (in preparation).
30. Lin, R.P. et al., 1995, Space Sci. Rev., 71, 125.
31. Lin, R.P. et al., 2002, Solar Physics, 210, 3-32.

32. Lin, R. P., Krucker, S., Holman, G. D., Sui, L., Hurford, G., and Schwartz, R. A. 2003, 28th international Cosmic Ray Conf., pp. 3207 - 3210.
33. Lin, L., Kashyap, V. L., Drake, J. J., DeLuca, E. E., Weber, M., and Sette, A. L. 2004, Proc. 13^{th} Cool Stars Workshop, Hamburg, eds. F. Favata et al.
34. Liu, C., Qiu, J. Gary, D.E., Krucker, S., Wang, H, 2004, ApJ 604, 442.
35. Masuda, S., Kosugi, T., Hara, H., Tsuneta, S., Ogawara, Y. 1994, Nature, 371, 495.
36. Mazzotta, P., Mazzitelli, G., Colafrancesco, S., & Vittorio, N., Ionization Balance for Optically Thin Plasmas, 1998, *A&AS*, 133, 403.
37. McKenzie, D.E., Hudson, H.S. 1999, ApJ, 519, L93.
38. Metcalf, T. R., Alexander, D., Hudson, H. S., and Longcope, D. W. 2003, ApJ, 595, 483 - 492.
39. Miller, J A. In: *High Energy Solar Physics: Anticipating HESSI*, ed by R. Ramaty & N. Mandzhavidze (ASP, San Francisco 2000), ASP Conf. Ser. 206, 145.
40. Morita, S., Uchida, Y., Hirose, S, Uemura, S., and Yamaguchi, T. 2001, Solar Physics, 200, 137 - 156.
41. Ohyama, M., & Shibata, K. 1998, ApJ, 499, 934.
42. Øieroset, M., Lin, R.P., Phan, T.D., Larson, D.E., and Bale, S.D., 2002, Physical Review Letters, 89, 19.
43. Phillips, K. J. H. 2004, ApJ, 605, 921 - 930.
44. Piana, M., Massone, A. M., Kontar, E. P., Emslie, A. G., Brown, J. C., and Schwartz, R. A., ApJL, 595, L127 - L130.
45. Priest, E.R. & Forbes, T.G, 2002, Astronomy Astrophysics Revs. 10, 313.
46. Qiu, J.; Lee, J.; Gary, D.E.; Wang, H., 2002, ApJ, 565, 1335.
47. Qiu, J., Liu, C., Gary D.E., Nita, G.M, Wang, H, 2004, ApJ (in press).
48. Ramaty, R., & Murphy, R. J. 1987, Space Sci. Rev., 45, 213.
49. Ramaty, R., Mandzhavidze, Kozlovsky, B., and Murphy, R. J. 1995, ApJL, 455, L193 - L196.
50. Saint-Hilaire, P. and Benz, A. O. 2002, Solar Physics, 210, 287 - 306.
51. Saint-Hilaire, P. and Benz, A. O. 2005, Astron. Astrophys., in press.
52. Sakao, T. 1994, PhD Thesis, University of Toko.
53. Sakao, T., Kosugi, T., Masuda, S., Yaji, K., Inda-Koide, M., and Makishima, K. 1995, Advances in Space Research, v. 17, no. 4/5, pp. 67 - 70.
54. Sakao, T., Kosugi, T., Masuda, S., 1998, in ASSL Vol. 229: Observational Plasma Astrophysics.
55. Schmahl, E. J. and Hurford, G. J., 2002a, Solar Physics, 210, 273 - 286.
56. Schmahl, E. J. and Hurford, G. J., 2002b, Adv. Space Res., 32, 2477 - 2482.
57. Schwartz, R.A. et al., 2002, Solar Physics, 210, 165.
58. Share, G. H., & Murphy, R. J. 1995, ApJ, 452, 933.
59. Share, G. H., et al. 2003, ApJL, 595, L85 - L88
60. Share, G. H., Murphy, R. J., Smith, D., M., Richard A. Schwartz, R. A., and Lin, R. P. 2004, ApJL, 615, L169 - L172.
61. Share, G. H. et al. 2005, in preparation.
62. Shibata, K., Masuda, S., Shimojo, M., Hara, H., Yokoyama, T., Tsuneta, S., Kosugi, T., Ogawara, Y. 1995, ApJ, 451, L83.
63. Smith, D.M.; Share, G.H.; Murphy, R.J.; Schwartz, R.A.; Shih, A.Y.; Lin, R.P., 2003, ApJL, 595, L81 - L84.
64. Sui, L, Holman, G. D., 2003, ApJL, 596, L251.

65. Sui, L., Holman, G. D., and Dennis, B. R., Krucker, S., Schwartz, R. A., and Tolbert, K. 2002, Solar Physics, 210, 245 - 259.
66. Sylwester, J., Gaicki, I., Kordylewski Z., et al., RESIK: A Bent Crystal X-ray Spectrometer for Studies of Solar Coronal Plasma Composition, 2004, Solar Physics, in press.
67. Tsuneta, S., Hara, H., Shimizu, T., Acton, L.W., Strong, K.T., Hudson, H.S., Ogawara, Y. 1992, PASJ, 44, L63.
68. Tsuneta, S. 1996, ApJ, 456, 840.
69. Veronig, A.M. & Brown, J.C, 2004, ApJL, 603, L117.
70. Woods, T. N., Eparvier, F. P., Fontenla, J., Harder, J., Kopp, G., McClintock, W. E., Rottman, G., Smiley, B., and Snow, M. 2004, Geophys. Res. Lett. 31, L10802.
71. Yokoyama, T., Akita, K., Morimoto, T., Inoue, K., Newmark, J. 2001, ApJ, 546, L69.